Desalination and Water Treatment
www.deswater.com
doi: 10.5004/dwt.2020.26058

198 (2020) 295–306
September

Simultaneous removal of endocrine-disrupting chemicals and microbes from waste-water using plant-mediated nickel oxide nanoparticles

Yaseen Ayub[a], Arsalan Sardar[a], Eder C. Lima[b], Rabia Nazir[c,*], Naveed-ul-Ihsan[a], Yasar Saleem[d], Raza Shah[e], Muhammad Abrar[f]

[a]*Department of Chemistry, Govt. Islamia College, Civil Lines Lahore-54000, Pakistan, emails: yaseenayub58@gmail.com (Y. Ayub), fahadsardar777@gmail.com (A. Sardar), naveedpu@hotmail.com (Naveed-ul-Ihsan)*
[b]*Institute of Chemistry, Federal University of Rio Grande do Sul (UFRGS), Av. Bento Goncalves 9500, P.O. Box: 15003, 91501-970 Porto Alegre, RS, Brazil, email: eder.lima@ufrgs.br (E.C. Lima)*
[c]*Applied Chemistry Research Centre, Pakistan Council of Scientific and Industrial Research Laboratories Complex, Ferozepur Road, Lahore-54600, Pakistan, email: rabiapcsir@yahoo.com (R. Nazir)*
[d]*Food and Biotechnology Research Centre, Pakistan Council of Scientific and Industrial Research Laboratories Complex, Ferozepur Road, Lahore-54600, Pakistan, email: ysaleem73@gmail.com (Y. Saleem)*
[e]*H.E.J. Research Institute of Chemistry, International Center for Chemical and Biological Sciences, University of Karachi, Karachi-75270, Pakistan, email: raza_shahm@yahoo.com (R. Shah)*
[f]*Department of Chemistry, Lahore Garrison University, Sector C, DHA Phase 6, Lahore, Pakistan, email: ibrarsattar@yahoo.com (M. Abrar)*

Received 16 February 2020; Accepted 2 May 2020

ABSTRACT

Wastewater treatment has always remained a precarious issue in the context of its environmental impacts and tackling of varied nature of contaminants. Plant-mediated NiO nanoparticles (G-NiO NPs) offer a way out to resolve these issues by presenting quick, cost-effective, less tedious and environmentally friendly approach to remove the potentially harmful multi-contaminants like endocrine-disrupting chemicals (for example reactive dyes, pesticides and phthalates) and microbial contaminants effectively. The formation of nanoparticles was confirmed by UV-Vis spectrophotometer, Fourier-transform infrared spectroscopy, X-ray diffraction, scanning electron scanning electron microscopy, energy-dispersive X-ray spectroscopy and AFM. The adsorption data was applied to various kinetic models, diffusion models and adsorption isotherms. Fitting of experimental data to these models showed best-fit models to be Avrami-fractional kinetic model and Liu adsorption model in all three cases (reactive red dye, bifenthrin and dioctyl phthalate) with adsorption capacities of 374.7, 34.85 and 323.59 mg g^{-1}, respectively. G-NiO NPs also proved potentially viable against *E. coli* with a 93% reduction in the microbial count.

Keywords: NiO nanoparticles; Reactive red dye; Bifenthrin; Dicotyl phthalate; *E. coli*; Kinetic models; Adsorption isotherms

1. Introduction

Treatment of waste-water has always been a problem of concern dealing with the diverse nature of microbial, organic, and inorganic contaminants leading to subsequent treatments passing through primary, secondary and tertiary processes [1]. Treatment and removal of endocrine-disrupting chemicals (EDC) from drinking, municipal and industrial waste-water have posed severe challenges because of their polar nature, the presence of acidic/basic functional groups, and occurrence at trace level <1 mg L^{-1}.

* Corresponding author.

Treatment of these usually requires energy-intensive procedures like advanced oxidation processes [2], but these can result in conversion to other carcinogenic compounds as a result of oxidation [3]. Furthermore, process requirements for removal of these contaminants are quite stringent [4], and these problems grow in by the presence of microbes in waste-water making water treatment protocols more complicated [5,6]. This scenario hence leads to substantial investment as well as the adaptation of tedious measures in context with stringent process requirements as well as treatment time. The situation can be handled and improved by use of nanomaterials enabling enhanced removal efficacy and reactivity which facilitates organic pollutants degradation and microbial decontamination [7]. Hence, in recent developments nanoparticles, nano-sorbents and nano-catalysts are extensively used for the removal of toxic chemicals and biological substances from waste-water, contaminated by heavy metals, nutrients, cyanide, organics compounds, algae, viruses, bacteria, parasites and antibiotics [8]. NiO NPs are suitable electron acceptor with high chemical stability and *p*-type semiconducting nature with band energy in the range of 1.5–5 eV, which makes it a good photocatalyst that can effectively break the bonds [9]. Hence, owing to these properties, NiO NPs have gained the attention of many researchers as a potential material to treat water contaminated with dyes [10–14], microbes [10,15], and heavy metals [16], etc.

Various routes are used to synthesize nanomaterials such as sol-gel [17,18], combustion [19], hydrothermal [20], co-precipitation [21] and green route method [22]. Among these, green route synthesis by plant extracts is the cost-effective, non-toxic, and best eco-friendly alternative method to synthesize nanoparticles as compared to other biological and traditional methods [23]. Henceforth, the present research was designed to synthesize NiO nanoparticles by using ethanolic extract of *Calotropis gigantea* leaves and exploring its potential for the treatment of water contaminated with multiple contaminants, that is, EDC and microbes.

2. Experimental setup

Analytical grade chemicals and solvents were used throughout the study. The solutions were prepared in lab prepared distilled water. $NiCl_2{\cdot}6H_2O$ and ethanol were procured from BDH Laboratory Supplies Poole, BH15 LTD, England, while reactive red 195 dye (96%) and dioctyl phthalate (99%) were obtained from PCSIR Lahore, Pakistan and used without further purification. pHs of solutions were adjusted by using 0.1 M solutions prepared from hydrochloric acid (PCSIR, Lahore, Pakistan) and sodium hydroxide (Sigma-Aldrich, Steinheim, Germany). Technical grade bifenthrin (91%) was provided by a local pesticide manufacturing company with established traceability to bifenthrin (99%) certified reference material provided by VWR Chemicals.

Leaves of *C. gigantea* were collected from botanical gardens of the University of the Punjab, Lahore, and verified by the Department of Botany, University of the Punjab, Lahore, Pakistan. The extract solutions were prepared in ethanol (Fluka) and distilled water.

2.1. Plant-mediated synthesis of NiO Nanoparticles (G-NiO NPs)

The G-NiO NPs synthesis was carried out using the ethanolic extract of leaves of *C. gigantea* by a modified process [24], as presented in Fig. 1. The system was modified to avoid the heat treatment required for the synthesis of plant extract and reduction of salt to Ni(0).

2.1.1. Preparation of ethanolic plant extract

Leaves of *C. gigantea* plant was consecutively washed with tap water and distilled water to remove mud and dust particles followed by drying under shade. The extract was prepared by dipping 300 g of washed dried crumbled leaves in 3 L of ethanol for 48 h with occasional shaking followed by filtration using Whatman® filter paper 41 (Buckinghamshire, UK). The filtrate was kept in the refrigerator at 4°C ± 2°C till further use.

2.1.2. Synthesis of G-NiO NPs

An aliquot of 100 mL of 0.5M $NiCl_2{\cdot}6H_2O$ was prepared in 1:1 water: ethanol mixture to synthesize G-NiO NPs. This solution was added to ethanolic plant extract (900 mL) and contents were stirred at 25°C for 24 h. 5 mL of sample was drawn at a defined interval from the reaction flask to perform UV-Vis spectroscopy to confirm the formation of nanoparticles. During reaction, change in color from light green to dark green was observed. After confirmation (by UV-Vis spectroscopy), the reaction mixture was rotary evaporated at 78°C until a thick, viscous material was obtained which was subsequently sintered at 600°C for 5 h; the resulting dark green powdered material was stored in screw-capped bottles for further studies.

2.2. Characterization

After synthesis, G-NiO NPs were characterized for their morphological, physical and chemical properties by double beam UV-Visible Spectroscopy (DB-20S), Fourier-transform infrared spectroscopy (FTIR) (Tensor-27), energy-dispersive X-ray spectroscopy (EDX), scanning electron microscopy (SEM) (S3700N, Hitachi, Japan), and X-ray diffraction (XRD) analysis (PANalytical) using standard procedures.

UV-Vis spectra were acquired in the range of 300–800 nm by using a quartz cuvette with a path of 10 mm. The samples that were drawn from the reaction mixture were diluted in ethanol at a concentration of 10^{-5} M before recording UV-Vis spectra.

2.2.1. Adsorption experiments of G-NiO NPs

The adsorption potential of G-NiO NPs towards EDC, that is, reactive dyes (reactive red 195, RR), pyrethroid pesticide (bifenthrin, BF) and phthalate (dioctyl phthalate, DOP) was assessed by using batch studies. The removal percentage and the amounts of adsorbates adsorbed at equilibrium time (adsorption capacity, $q_{e,\exp}$) were calculated using Eqs. (1) and 2 (Table 1). Various other models and isotherms were also applied to the adsorption experiments performed, as mentioned in Table 1, along with their equations [Eqs. (3)–(11)].

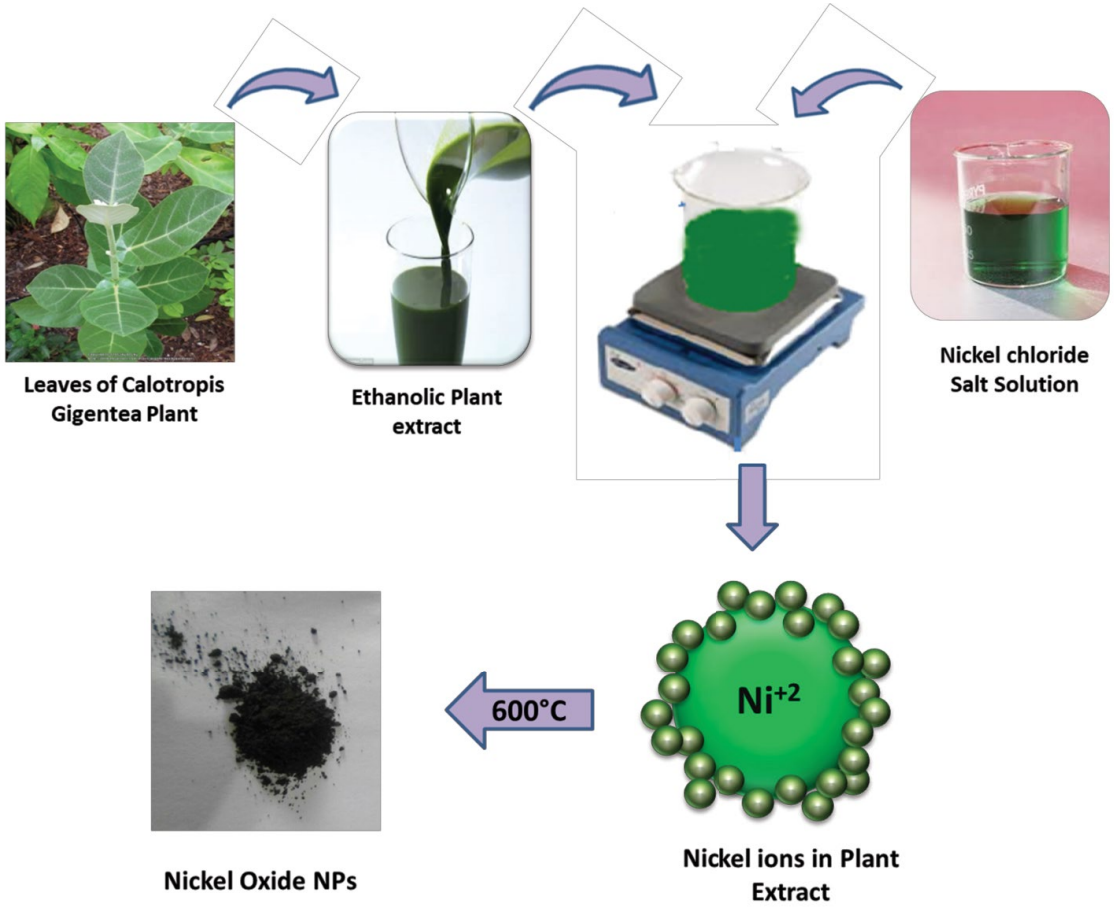

Fig. 1. Graphical abstract for the plant-mediated synthesis of G-NiO NPs.

2.2.2. Reactive red 195 dye

To study the ability of G-NiO NPs for removal of dyes from the binary system, RR was chosen as a test contaminant along with four parameters, that is, contact time (min), temperature (K), initial pH, and RR concentration (mg L^{-1}) were selected. For this, RR (100–800 mg L^{-1}) was allowed to remain in contact with 0.1 g nano-catalyst for definite time and temperature at different pH in order to achieve maximum adsorption of RR onto the nano-adsorbent surface. After a specific time, the contents were cannula filtered, and the filtrate was checked for dye concentration using a UV-Vis spectrophotometer at 541 nm [31].

2.2.3. Bifenthrin

The adsorption potential of G-NiO NPs towards pesticides was also studied by choosing bifenthrin (BF) as a test contaminant. For the purpose working solution of BF (10–50 mg L^{-1}) was allowed to remain in contact with G-NiO NPs (0.1 g) at room temperature for different timings (2–60 min), and the resulting contents were cannula filtered. The pH and temperature effects were not studied owing to possible chances of degradation of BF.

BF in filtrate was extracted using liquid-liquid extraction. The filtrate was transferred to separating funnel, followed by the addition of 1 mL of 10% NaCl to enhance the extraction efficacy. *n*-Hexane was used as extracting solvent and extraction was performed thrice with 10 ml × 1 and 5 ml × 2. *n*-Hexane layer was transferred to the rotary evaporator flask by passing it through a layer of anhydrous sodium sulfate (pretreated at 600°C). The volume was reduced to approximately 1 mL and re-constituted to 5 mL using anhydrous sodium sulfate treated *n*-hexane. Working standards were also extracted by the same method (to accommodate method recovery) and analyzed using GC-ECD (Varian CP-3800) equipped with a DB-5 column with a 0.1 µm internal diameter and 30 m length. The injector and detector temperature were set at 250°C. The oven temperature ramping was set as follows: Initial temperature 100°C held for 2 min; ramp to 200 @ 50°C min^{-1} held for 2 min; ramp to 230°C @ 5°C min^{-1} held for 2 min; ramp to 250°C @ 50°C min^{-1} held for 5 min.

The concentration of the BF in the treated sample was calculated from the GC data by using the following equation:

$$C_s = C_{std} \times \frac{A_s}{A_{std}} \times \frac{V_{std}}{V_s} \quad (1)$$

where C_s and C_{std} are the concentrations of BF in the treated sample and standard, A_s and A_{std} are the peak areas of BF in treated and standard samples as obtained from GC

chromatogram, and V_s and V_{std} are the injected volumes of treated sample and standard solution which in this case is kept constant (1 μL).

2.2.4. Dioctyl phthalate

DOP, a carcinogenic chemical, removal was also studied by using prepared G-NiO NPs. For the purpose working solution of DOP (50–400 mg L^{-1}) was allowed to remain in contact with G-NiO NPs (0.1 g) at room temperature for different timings (5–70 min) and the resulting contents were cannula filtered. The pH and temperature effects were not studied owing to possible chances of degradation of DOP.

The DOP in the filtrate (sample) and working standards were extracted using liquid-liquid extraction using the same protocol as was in the case of BF. The extracted samples were analyzed using GC-FID (Agilent 7890B) with ALS equipped with an HP-5 column with a 0.1 μm internal diameter and 30 m length. The injector and detector temperature were set at 300°C. The oven temperature ramping was set as follows: initial temperature of 150°C held for 5 min then ramp to 280°C at 20°C min^{-1} held for 5 min at the final temperature. The adsorbed percentage was calculated from the GC data by using Eqs. (12) and (2).

2.2.5. Antimicrobial activity of G-NiO NPs

The antibacterial activity of G-NiO NPs was tested against bacterial growth of *E. coli* that is used as a representative gram-negative bacterium. Aliquots of 2 mL of *E. coli* bacterial agar was added in 2 L autoclaved distilled water and kept in a refrigerator at 4°C ± 2°C for further use. 50 mL of this simulated sample was taken in an Erlenmeyer flask and allowed to remain in contact with 0.1 g of G-NiO NPs for different time intervals (10, 30, 50, 70, 90, and 110 min). The contents were cannula filtered, and the filtrate was placed in tightly packed rubber septum bottles and kept in a refrigerator at 4°C ± 2°C. For cell calculation 0.5 μL of treated *E. coli*, strain solution was injected on a hemocytometer, stained with safranin and crystal violet, and placed on the microscope for studying the % removal.

Percentage (%) removal of cells was determined by comparing each sample with untreated one.

$$R(\%) = \frac{N_t}{N_i} \times 100 \quad (2)$$

where N_t and N_i are the number of cells after and before treatment, respectively.

3. Results and discussion

The ethanolic extract of plant leaves of *C. gigantea* is a good source of active organic compounds such as proteins, amino acids, glycosides, flavonoids, etc. that can act as good reducing agents and result in metal nanoparticles synthesis [32–34].

The extract was employed in essence to exploit its perspective as a potential bio-factory for the synthesis of G-NiO NPs. *C. gigantea* leaves extract has a rich source of active organic compounds such as proteins, amino acids, glycosides, flavonoids, etc. Therefore, naturally occurring plant metabolites have a favorable effect on NPs synthesis by acting as good reducing as well as capping/chelating agents [24,35,36]. During reaction, conversion of Ni(II) to Ni(0) takes place, which is evidenced by UV-Vis spectra. The UV-Vis spectra (Fig. 2) shows minimization in $NiCl_2$ peak recorded at 661 cm^{-1}. Earlier studies have shown that in green synthesis, the reduction and conversion of metallic ions to zerovalent nanoparticles is assisted by the formation of metal chelated complexes with the plant phytochemicals, which can be easily decomposed at temperatures ≥ 400°C leading to the formation of metal oxide nanoparticles [24,35].

3.1. Characterization

3.1.1. Fourier-transform infrared spectroscopy

The FTIR spectra of *C. gigantea* and G-NiO NPs are presented in Fig. 3a. In *C. gigantea* spectra peaks appeared at 3,317; 2,981 and 2,359 cm^{-1} due to the presence of –OH, $–CH_2$, and $–CH_3$. The peak at 1,645 cm^{-1} was attributed to stretching vibrations of C=O containing compounds while the ones appearing at 1,454 and 1,386 cm^{-1} are ascribed to –CH bending vibrations. The bands at 1,085; 1,044–1,016; 878 and 694–609 cm^{-1} are indicative of C–O–C, C–O stretching, bending vibrations of C–H aromatic compounds and bending vibration of C–O–O aromatic compounds, respectively [37].

The majority of the peaks available in *C. gigantea* spectra are not evidenced in G-NiO NPs spectra (Fig. 3a) because of the decomposition of organic moieties owing to the sintering process. Few peaks appear at 3,324; 2,034 and 681 cm^{-1}, which correspond to a hydroxyl group (–OH) stretching probably due to moisture in the sample while the peak at 1,606 cm^{-1} refers to stretching vibration of the C=O group [38]. The C–O–C stretching peak is evidenced at 1,156.63 cm^{-1}. The peak of Ni–O stretching observed below 1,000 cm^{-1}. The FTIR spectrum shows the characteristic peak at 681 and 642 cm^{-1} corresponding to the metal-oxygen (NiO) stretching vibration [24,39].

3.1.2. Powder XRD

The powder XRD analysis was also performed to elucidate the crystalline structure of G-NiO as well as its phase analysis. The XRD spectra presented in Fig. 3b displayed five-strong diffraction peaks corresponding to hkl values of [2 2 2], [4 0 0], [4 4 0], [6 2 2] and [4 4 4] which confirms the formation of nickel oxide nanoparticles. The diffraction peaks showed good agreement with the cubic structure (JCPDS: 01–089–5881), as shown in the inset of Fig. 3b inset.

3.1.3. SEM/EDX and AFM

SEM micrograph and EDX analysis (presented in Fig. 4) were carried out to determine the shape, morphology, elemental composition and purity of synthesized G-NiO NPs. Fig. 4a points to the formation of spongy material with a porous structure. The agglomeration of the particles is indicated from the SEM image which is in line with earlier studies [24]. Such agglomeration, which results in bigger particles, is

Table 1
Equations used for the adsorption and various models applied

Eq. No.	Description	Equation	Reference
1.	Removal percentage (%)	$R(\%) = \frac{C_i - C_t}{C_i} \times 100$	[25]
2.	Adsorption capacity (mg g^{-1})	$q_{e,\exp} = \frac{C_f\left(\text{mg L}^{-1}\right)}{W(\text{g})} \times V(\text{L})$	
3.	Pseudo-first-order	$q_t = q_e\left[1 - \exp\left(-k_{1\text{NL}} \cdot t\right)\right]$	[26]
4.	Pseudo-second-order	$q_t = \frac{k_{2\text{NL}} \cdot q_e^2 \cdot t}{1 + q_e \cdot k_2 \cdot t}$	
5.	Avrami kinetic model	$q_t = q_e\left\{1 - \exp\left[-\left(k_{\text{AV}} t\right)\right]^n\right\}$	[27]
6.	Chi-square	$\chi^2 = \sum \frac{\left(q_{e,\exp} - q_{e,\text{cal}}\right)^2}{q_{e,\text{cal}}^2}$	[28]
7.	Particle diffusion	$\ln\left(1 - \frac{C_t}{C_e}\right) = -k_p t$	[29]
8.	Inter-particle diffusion	$q_t = k_{\text{id}} t^{0.5} + C_i$	[27]
9.	Langmuir adsorption isotherm	$q_e = \frac{q_m \times K_L \times C_e}{1 + K_L \times C_e}$	
10.	Freundlich adsorption isotherm	$q_e = K_F \times C_e^{1/n_F}$	[30]
11.	Liu adsorption isotherm	$q_e = \frac{q_m \times \left(K_g \times C_e\right)^{n_L}}{1 + \left(K_g \times C_e\right)^{n_L}}$	

R (%) = percentage removal (%); $q_{e,\exp}$ (mg g^{-1}) = contaminant adsorbed per gram of adsorbate; C_i (mg L^{-1}) = initial concentration of adsorbate; C_t (mg L^{-1}) = concentration of adsorbate remaining in the solution after time, t (min); C_f (mg L^{-1}) = final concentration of adsorbate taken up by adsorbent calculated by (C_i – C_t); V (L) = volume of solution; W (g) = weight of the adsorbent; q_e (mg g^{-1}) = amount of adsorbent at equilibrium; q_t (mg g^{-1}) = amount of adsorbent at time t (min); k_1 (min^{-1}) and k_2 (g mg^{-1} min^{-1}) are the rate constants for pseudo-first-order and pseudo-second-order, respectively; k_{id} (mg g^{-1} min$^{-0.5}$) = rate parameter of stage i; C_i = thickness of boundary layer; k_p = rate parameter for the particle diffusion; q_m (mg g^{-1}) = maximum adsorption capacity, K_L (L mg^{-1}) and K_F (mg g^{-1} (mg L^{-1})$^{-1/nF}$) are Langmuir and Freundlich constants for determining the rate of adsorption; n_F = Freundlich dimensionless exponent. K_g (L mg^{-1}) and n_L are Liu constant and exponent, respectively.

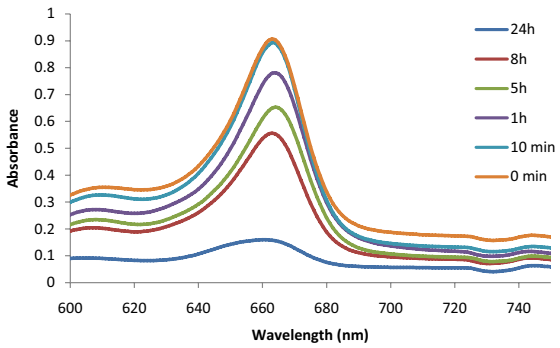

Fig. 2. UV-Visible spectra of synthesized G-NiO NPs showing the change with the progress of the reaction.

usual for nanoparticles because of their small size and high surface energy [10]. Ni and O peaks are majorly conspicuous in the EDX spectrum (Fig. 4b), with a weight % ratio of 56.05% and 21.66%, respectively. The quantitative data confirms the presence of corresponding elements with the presence of some impurities like Cl, which is contributed from the use of nickel chloride as a reactant. Other elements Na, Mg, Al, and K, may-be due to the presence in leaves of *C. gigantea* plant.

AFM analysis also confirmed the agglomeration of the nanoparticles in the prepared sample. Images 3D and 2D (Figs. 5a and b) also points to the agglomeration of nanoparticles as was evidenced by SEM image (Fig. 4a). Some needles like structure and oblong-shaped particles are also visible in the 2D image (Fig. 5b) with smaller sizes.

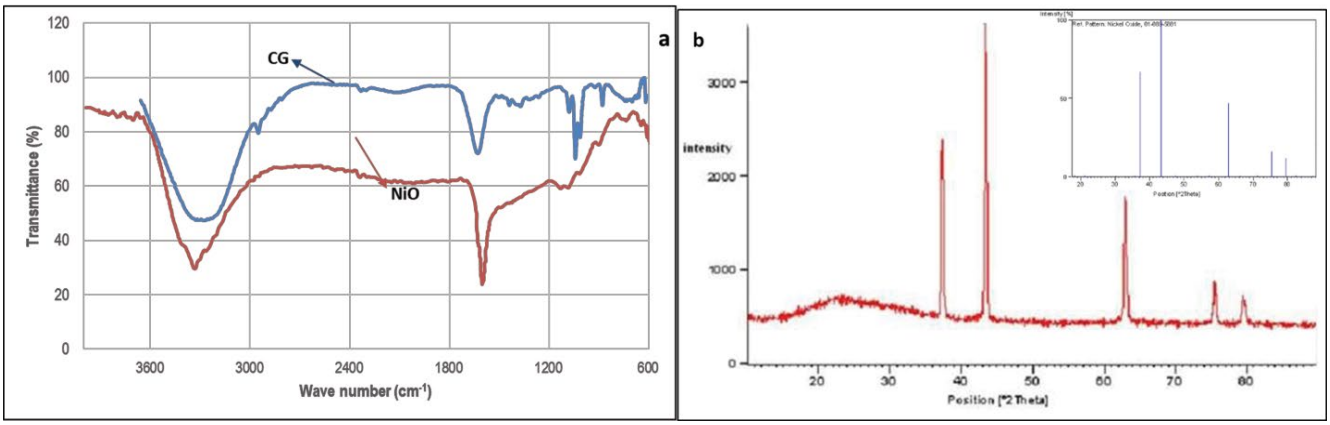

Fig. 3. (a) FTIR spectrum of *C. gigantea* extract and G-NiO NPs and (b) powder XRD spectra of G-NiO NPs showing matching with JCPDS: 01-089-5881 (inset).

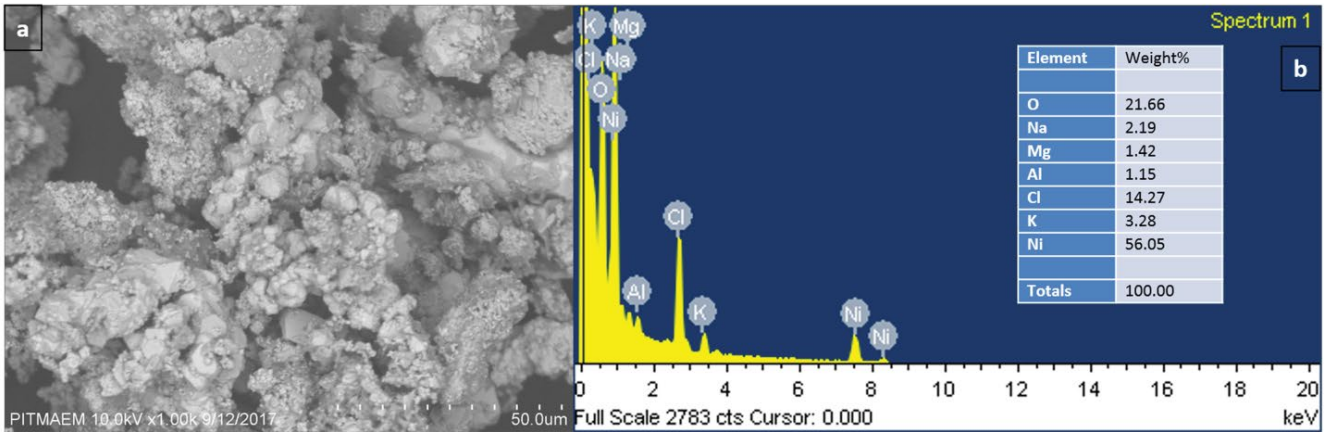

Fig. 4. G-NiO NPs (a) SEM micrograph and (b) EDX spectrum along with elemental composition in the inset.

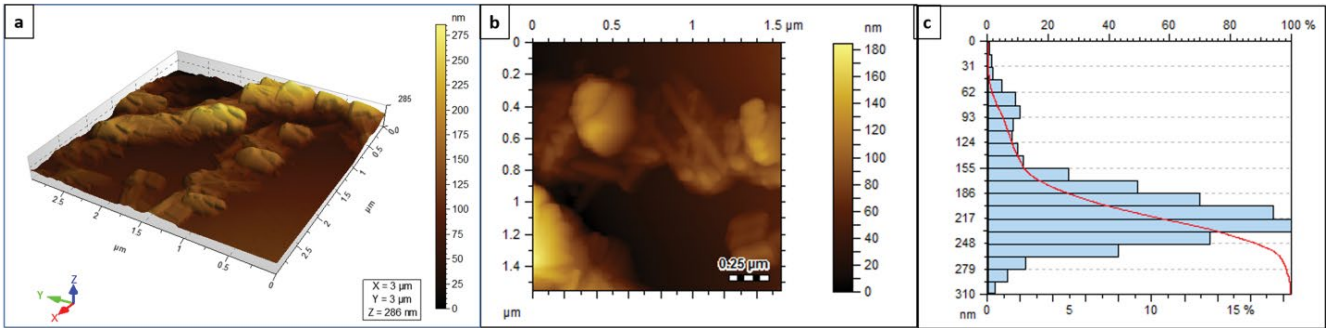

Fig. 5. AFM images of G-NiO NPs (a) 3D, (b) 2D, and (c) particle size distribution histogram.

The particle size range, as depicted from the histogram (Fig. 5c), is 31 nm to 310 nm with an average particle size of 232 nm.

3.2. Adsorption potential

The G-NiO NPs produced from *C. gigantea* plant extract were used for the removal of reactive red 195 dye, bifenthrin and dioctyl phthalate in an aqueous medium.

3.2.1. Effect of contact time, kinetic and diffusion models

The time for which adsorbent remains in contact with the adsorbent had a high impact on the adsorption efficacy. With an increase in contact time, there is an increase in adsorption of the adsorbates until it achieves equilibrium (Fig. 6). The kinetic models were applied to the data at a fixed temperature (i.e., RT) to predict the sorption kinetics for the G-NiO NPs. Pseudo-first-order, pseudo-second-order

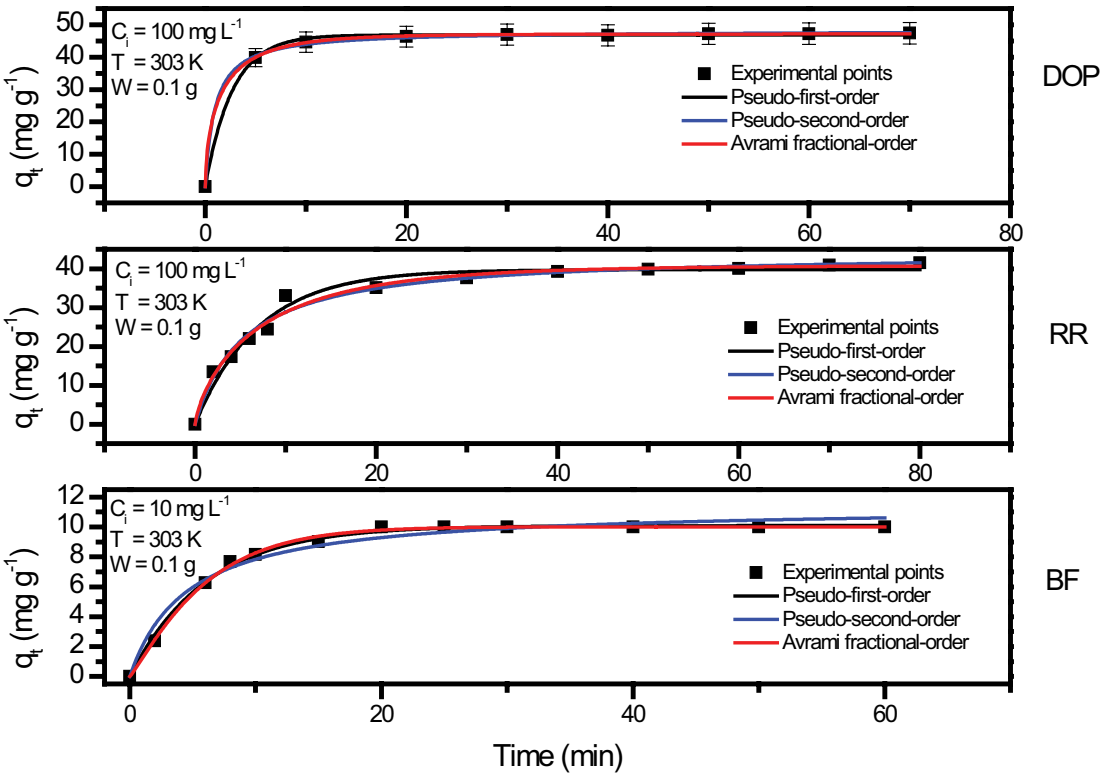

Fig. 6. Fitting of kinetic models to G-NiO NPs for adsorption of DOP, RR, and BF.

and Avrami-fractional-order kinetic models were applied in non-linear form, and best fit models in both cases were predicted from high R^2, reduced χ^2, smaller standard deviation (SD) and the difference between experimental and calculated q_e. The parameters derived for these models are given in Table 2. Also, by interpolation in the fitted kinetic curve, it was calculated $t_{0.5}$ and $t_{0.95}$ is the time to attain 50% and 95% of the saturation. These values are also reported in Table 2. Considering the values of SD, the model that presented the lower values of SD for the three adsorbates was the Avrami-fractional kinetic model. Therefore, statistically, this kinetic adsorption model is the most suitable model to describe the kinetics of adsorption.

It is possible to infer that the kinetics of DOP is the fastest one, followed by BF and them by RR, by comparing the values of $t_{0.5}$ and $t_{0.95}$ of the three adsorbates. This is probably associated with the dimension of the chemical molecules.

Particle diffusion [Eq. (8)] and Inter-particle diffusion [Eq. (9)] models were also applied to get insight into the diffusion process; the fitting parameters obtained are tabulated in Table 2. The plot of the particle diffusion model based on Chanda plots, that is, ln $(1 - C_t/C_e)$ vs. t [Eq. (8); Fig. 7] [40,41] gives a straight line which refers to the adsorption phenomenon being controlled by particle diffusion [42]. Further, investigation using inter-particle diffusion model (Fig. 7, Table 2) suggests, in all the three cases (RR, BF, DOP), that different sorption phenomena are occurring as the plot fitted to two straight lines pointing to the multi-step adsorption [43].

The maximum adsorption for the RR, BF and DOP onto G-NiO NPs was achieved 10, 20, and 30 min.

3.2.2. *Effect of temperature and initial pH*

Temperature and initial pH of the solution has a considerable effect on the adsorption process, as also reported in previous studies [13, 14,44]. Fig. 8 presents the effects of varying initial pH and temperature on the adsorption of RR onto G-NiO NPs.

Adsorption of dye (100 mg L^{-1}) was studied in an amplitude temperature of 30°C–60°C in the presence of G-NiO NPs (2 g L^{-1}). The adsorption efficiency of dye was observed to decrease slightly with escalating temperature, that is, 67% to 63% (Fig. 8). Therefore, further studies were performed at room temperature, that is, 303 K. In contrast to temperature, pH had a considerable effect on the removal percentage of RR (Fig. 8), resulting in almost complete removal of the dye at pH 11, that is, 98%.

For BF and DOP, the effect of temperature and pH was not studied owing to their possible degradation and formation of other degradation products as a result of changes in pH and temperature.

The decrease in adsorption with an increase in temperature is indicative of the exothermic process of adsorption. A similar response was also observed in dye adsorption studies on NiO. The phenomenon was attributed to enhancement in dye mobility and solubility, as well as an increase in the diffusion of dye molecules into the adsorbent porous structure [14].

In the case of pH, dye molecules (RR) behaves as cationic when the solution pH is acidic and anionic when pH is basic. This behavior results in its high adsorption in case of low solution pH and high basic pH. Furthermore,

Table 2
Adsorption kinetics and diffusion models fitting parameters for RR, BF and DOP adsorption on G-NiO NPs along with the goodness of fit parameters

Model	Parameter	Value (RR)	Value (BF)	Value (DOP)
Avrami-fractional order	$q_{e,cal}$ (mg g^{-1})	40.772	10.013	47.147
	k_{1NL} (min^{-1})	0.131	0.164	0.562
	N	0.761	1.129	0.610
	R^2_{adj}	0.9836	0.9975	0.9998
	SD	1.674	0.169	0.208
	Reduced χ^2	2.802	0.0284	0.043
	$t_{0.5}$ (min)	4.721	4.417	0.9763
	$t_{0.95}$ (min)	32.35	16.15	10.74
Pseudo-first-order (non-linear)	$q_{e,cal}$ (mg g^{-1})	39.759	10.093	46.862
	k_{1NL} (min^{-1})	0.143	0.164	0.371
	R^2_{adj}	0.9778	0.9959	0.9988
	SD	1.952	0.213	0.542
	Reduced χ^2	3.809	0.045	0.293
	$t_{0.5}$ (min)	4.859	4.238	1.866
	$t_{0.95}$ (min)	21.00	18.32	8.064
Pseudo-second-order (non-linear)	$q_{e,cal}$ (mg g^{-1})	44.290	11.418	48.233
	k_{2NL} (min^{-1})	0.00421	0.019	0.0213
	R^2_{adj}	0.9842	0.9743	0.9993
	SD	1.644	0.537	0.398
	Reduced-χ^2	2.705	0.289	0.159
	$t_{0.5}$ (min)	5.365	4.579	0.975
	$t_{0.95}$ (min)	–	–	18.528
Particle diffusion	k_p (mg g^{-1}min^{-1})	–1.442	–1.284	–1.077
	R^2_{adj}	0.9580	0.6367	0.8549
Intra-particle diffusion	k_{id1} (mg g^{-1} min$^{-0.5}$)	10.446	2.406	2.049
	C_{i1} (mg g^{-1})	–2.710	–0.045	36.600
	R^2_{j1ad}	0.8981	0.8998	0.7491
	k_{id2} (mg g^{-1} min$^{-0.5}$)	1.456	3.808	0.167
	C_{i2} (mg g^{-1})	29.04	9.997	45.945
	R^2_{2adj}	0.9493	0.2017	0.5441

the sites of adsorbent also behave differently at acidic and basic pH. Both these factors combine to determine the behavior of dye adsorption when the pH of the solution is changed [14].

3.2.3. Effect of the initial concentration of adsorbates and adsorption isotherms

Effect of initial concentration of RR (100–800 mg L^{-1}), BF (10–50 mg L^{-1}) and DOP (50–400 mg L^{-1}) on adsorption efficiency of G-NiO NPs was assessed by varying concentrations (Fig. 9). The increase in adsorption capacity with an increase in concentration is typical behavior for adsorption, as was observed in previous studies [13,14]. At low adsorbate concentrations, there are few numbers of adsorbate molecules available for adsorption on the specific number of adsorbent sites resulting in low adsorption capacity, that is, the amount of adsorbate per gram of adsorbent. As the concentration of adsorbate increases, the adsorbant specific sites become saturated and the exchange sites are filled resulting in the high adsorption capacity as the overall amount of adsorbate adsorbed per gram of adsorbent increases [45].

The best-fitting model is decided based on high R^2 value, smaller SD, and reduced-χ^2 values (Table 3). On this basis, Liu adsorption model in all three cases (Fig. 9) comes out to be the best-fit model, which indicates that adsorbents' active sites are not of the same energy [46]. This is highly plausible because of agglomeration, as indicated by SEM (Fig. 4) and AFM (Fig. 5). The maximum adsorption capacities as determined from the best fit model were 374.7, 34.85, and 323.59 mg g^{-1} for RR, BF and DOP, respectively.

The results revealed that under optimal conditions of pH 7 and room temperature, G-NiO NPs dosage of 2 g L^{-1} and contact time of 10, 20 and 30 min at concentration of 600, 30 and 300 mg L^{-1}, the maximum adsorption capacity (q_m) of RR, BF and DOP adsorption on G-NiO NPs was 374.7, 34.8 and 323.6 mg g^{-1}.

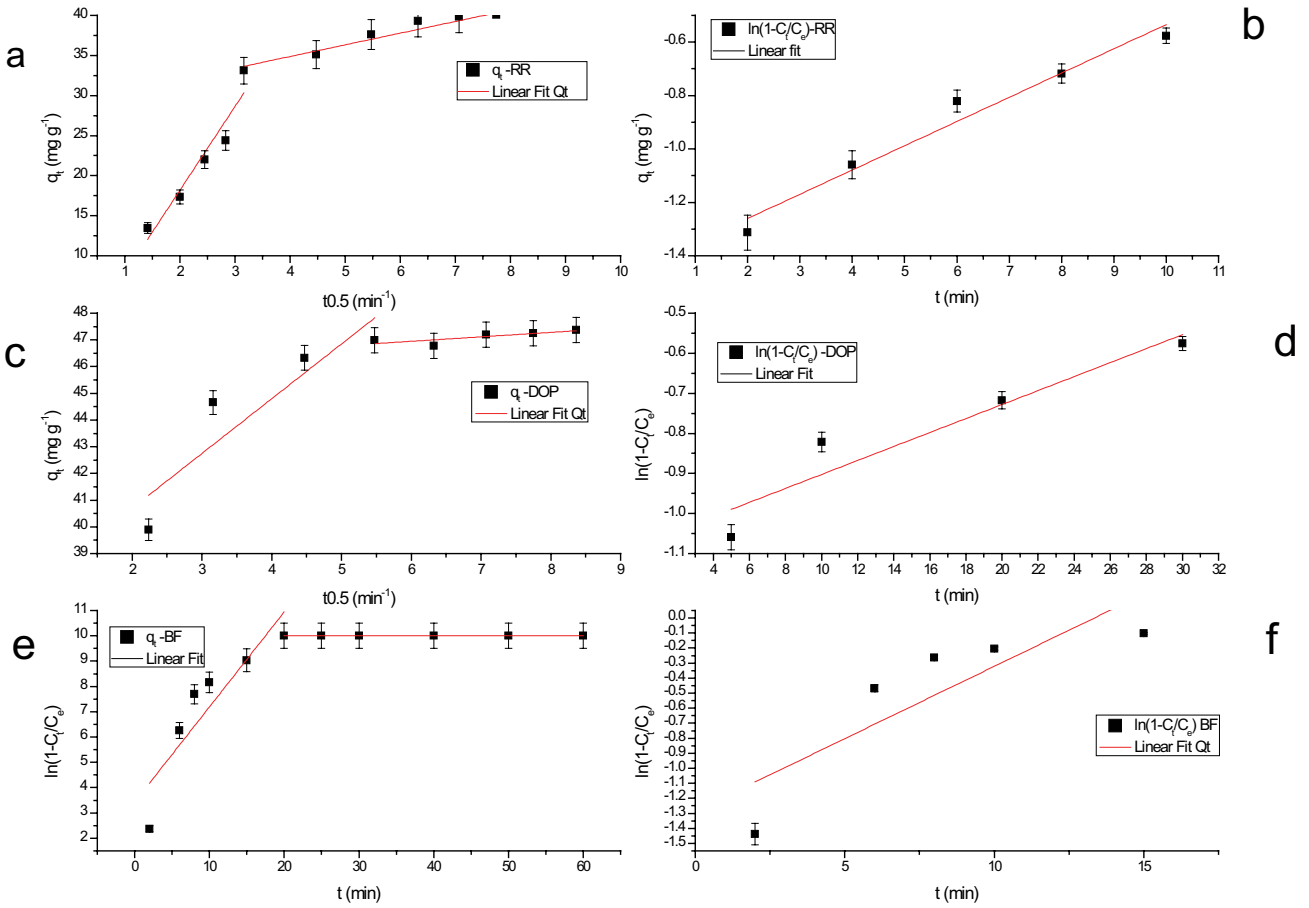

Fig. 7. Fitting of interparticle (q_t vs. $t_{0.5}$) and particle diffusion (ln(1 – C_t/C_e vs. t)) models to adsorption of RR (a,b), DOP (c, d) and BF (e, f), respectively onto G-NiO NPs.

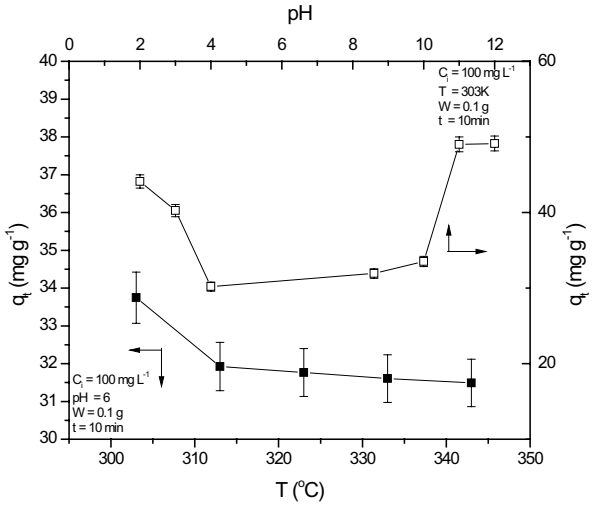

Fig. 8. Effect of adsorption of RR on G-NiO NPs with temperature (■) (primary *x*- and *y*-axis) and initial pH (○) (secondary *x*- and *y*-axis).

3.3. Antimicrobial activity

The antimicrobial activity of G-NiO NPs was tested against gram-negative bacteria, that is, *E. coli* for a period of 10–110 min, as shown in Fig. 10. The reduction reached 93% within 2 h with just 0.1 g of the G-NiO NPs. Earlier studies have also shown the antibacterial potential of the NiO nanoparticles and attributed the high antimicrobial activity to a smaller size of the particles that help in easy diffusibility of particles into the cell wall along with enhancing the electrostatic interaction between the metal ions and the cell wall. It was also proposed that these particles produced reactive species (OH^-, H_2O_2, O_2^{2-}) that can damage the cell membrane resulting in the increased antibacterial potential of the nanoparticles [47–49].

4. Conclusion

Calotropis gigentea leaves based route was adopted for the synthesis of cubic phase NiO nanoparticles. The simple route ensures the formation of nanoparticles that were found useful in the effective removal of three potential organic pollutants, that is, dyes (reactive red 195 dye), pesticide (bifenthrin), and phthalate (dioctyl phthalate) in maximum 30 min and at room temperature. The adsorption data were fitted to various adsorption and kinetic models, and the fitting results showed that the adsorption is best described by the Avrami-fractional kinetic model and Liu adsorption model. The results suggested that the G-NiO

Table 3
Langmuir, Freundlich and Liu adsorption models constant as applied to RR, BF and DOP adsorption on G-NiO NPs

Model	Parameter	Value (RR)	Value (BF)	Value (DOP)
Langmuir	K_L (L mg^{-1})	0.0013	0.0261	7.99×10^{-4}
	q_m (mg g^{-1})	617.80	59.122	682.838
	R^2_{adj}	0.9842	0.9136	0.9929
	SD (mg g^{-1})	10.071	2.432	4.905
	Reduced χ^2	101.419	5.915	24.063
Freundlich	K_F (mg g^{-1} (mg L^{-1})$^{-1/nF}$)	2.435	3.282	1.034
	n_F	1.040	1.667	1.177
	R^2_{adj}	0.9665	0.8921	0.999
	SD (mg g^{-1})	14.653	3.072	1.161
	Reduced χ^2	214.715	9.440	132.151
Liu	q_m (mg g^{-1})	374.738	34.851	323.596
	K_g (L mg^{-1})	0.002	0.061	0.002
	n_L	1.443	2.163	1.269
	R^2_{adj}	0.9918	0.9676	0.9947
	SD (mg g^{-1})	7.226	1.488	4.241
	Reduced χ^2	52.216	2.216	17.992

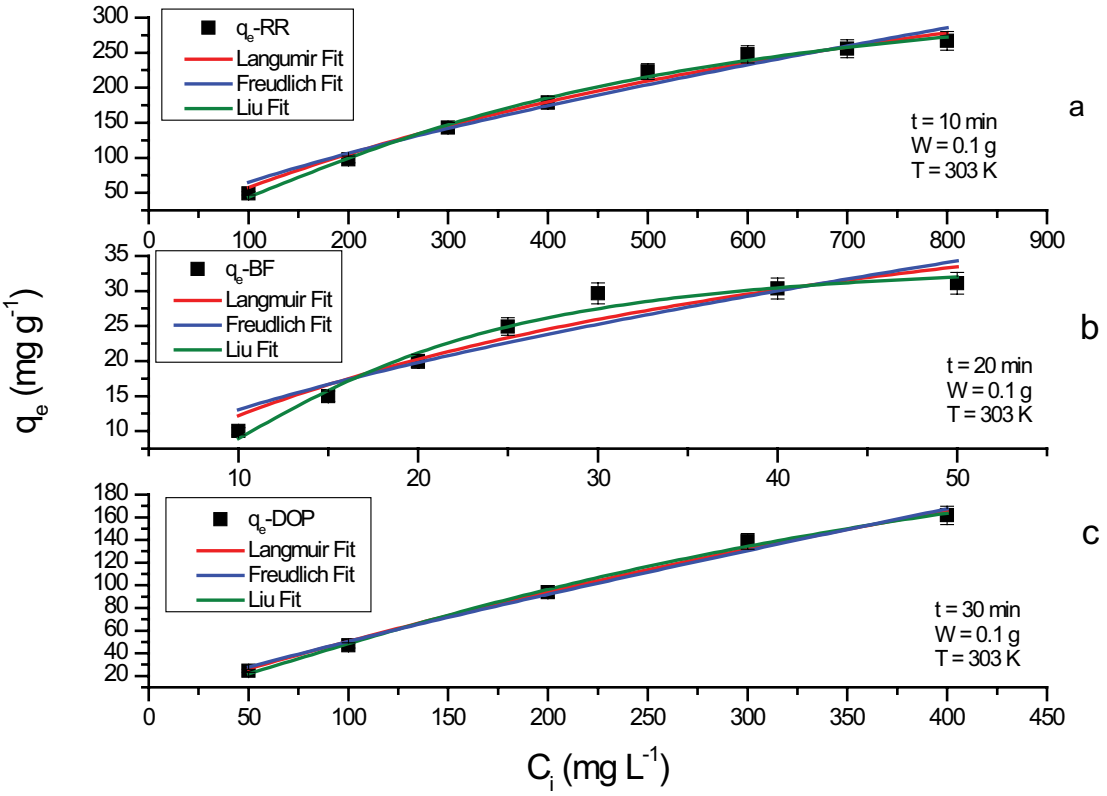

Fig. 9. Fitting of adsorption models to G-NiO NPs for adsorption of RR (a), BF (b), and DOP (c).

NPs can remove multiple contaminants in less time and appreciable adsorption capacities (374.7 (RR), 34.85 (BF) and 323.59 (DOP) mg g^{-1}). G-NiO NPs had also shown significant antimicrobial potential and ensured almost complete removal of *E. coli*.

Acknowledgments

The authors thank the Pakistan Council of Scientific and Industrial Research Laboratories Complex, Lahore, Pakistan and National Council for Scientific and Technological Development (CNPq, Brazil) for financial support and

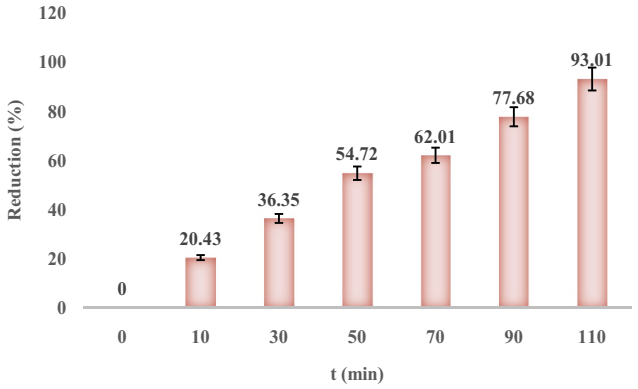

Fig. 10. Antimicrobial potential of G-NiO NPs towards *E. coli* at different contact times.

sponsorship. We are also grateful to ChemAxon for giving us an academic research license for the Marvin Sketch software, Version 19.8.0 (http://www.chemaxon.com), 2019 used for molecule physical-chemical properties.

References

[1] I. El Saliby, H.K. Shon, J. Kandasamy, S. Vigneswaran, Nanotechnology for wastewater treatment: in brief, Encycl. Life Support Syst., 7 (2008) 1–15.
[2] E.J. Rosenfeldt, K.G. Linden, Degradation of endocrine disrupting chemicals bisphenol A, ethinyl estradiol, and estradiol during UV photolysis and advanced oxidation processes, Environ. Sci. Technol., 38 (2004) 5476–5483.
[3] S.A. Snyder, P. Westerhoff, Y. Yoon, D.L. Sedlak, Pharmaceuticals, personal care products, and endocrine disruptors in water: implications for the water industry, Environ. Eng. Sci., 20 (2003) 449–469.
[4] A.C. Johnson, J.P. Sumpter, Removal of endocrine-disrupting chemicals in activated sludge treatment works, Environ. Sci. Technol., 35 (2001) 4697–4703.
[5] M.A. Mahmood, S. Baruah, A.K. Anal, J. Dutta, Heterogeneous photocatalysis for removal of microbes from water, Environ. Chem. Lett., 10 (2012) 145–151.
[6] R.L. Rajala, M. Pulkkanen, M. Pessi, H. Heinonen-Tanski, Removal of microbes from municipal wastewater effluent by rapid sand filtration and subsequent UV irradiation, Water Sci. Technol., 47 (2003) 157–162.
[7] X. Qu, P.J. Alvarez, Q. Li, Applications of nanotechnology in water and wastewater treatment, Water Res., 47 (2013) 3931–3946.
[8] D.K. Tiwari, J. Behari, P. Sen, Application of nanoparticles in waste water treatment, World App. Sci. J., 3 (2008) 417–433.
[9] Z. Sabouri, A. Akbari, H.A. Hosseini, M. Khatami, M. Darroudi, Egg white-mediated green synthesis of NiO nanoparticles and study of their cytotoxicity and photocatalytic activity, Polyhedron, 178 (2020) 114351.
[10] S.A. Bhat, F. Zafar, A.H. Mondal, A. Kareem, A.U. Mirza, S. Khan, A. Mohammad, Q.M.R. Haq, N. Nishat, Photocatalytic degradation of carcinogenic Congo red dye in aqueous solution, antioxidant activity and bactericidal effect of NiO nanoparticles, J. Iran. Chem. Soc., 17 (2020) 215–227.
[11] M.Z. Bani-Fwaz, A.A. El-Zahhar, H.S. Abd-Rabboh, M.S. Hamdy, M. Shkir, Synthesis of NiO nanoparticles by thermal routes for adsorptive removal of crystal violet dye from aqueous solutions, Int. J. Environ. Anal. Chem., (2019) 1–19, https://doi.org/10.1080/03067319.2019.1678599.
[12] Al-Aoh, A. Hatem, Adsorption performances of nickel oxide nanoparticles (NiO NPs) towards bromophenol blue dye (BB), Desal. Water Treat., 110 (2018) 229–238.
[13] A. Darwish, M. Rashad, H.A. AL-Aoh, Methyl orange adsorption comparison on nanoparticles: Isotherm, kinetics, and thermodynamic studies, Dyes Pigm., 160 (2019) 563–571.
[14] H.A. Al-Aoh, I.A. Mihaina, M.A. Alsharif, A. Darwish, M. Rashad, S.K. Mustafa, M.M. Aljohani, M.A. Al-Duais, H. Al-Shehri, Removal of methylene blue from synthetic wastewater by the selected metallic oxides nanoparticles adsorbent: equilibrium, kinetic and thermodynamic studies, Chem. Eng. Commun., (2019) 1–17, https://doi.org/10.1080/00986445.2019.1680366.
[15] G. Ilbeigi, A. Kariminik, M.H. Moshafi, The antibacterial activities of NiO nanoparticles against some gram-positive and gram-negative bacterial strains, Int. J. Basic Sci. Med., 4 (2019) 69–74.
[16] M.R. Abukhadra, M.A. Sayed, A.M. Rabie, S.A. Ahmed, Surface decoration of diatomite by Ni/NiO nanoparticles as hybrid composite of enhanced adsorption properties for malachite green dye and hexavalent chromium, Colloids Surf., A, 577 (2019) 583–593.
[17] N.N.M. Zorkipli, N.H.M. Kaus, A.A. Mohamad, Synthesis of NiO nanoparticles through sol-gel method, Procedia Chem., 19 (2016) 626–631.
[18] S. El-Sheikh, R. Mohamed, O. Fouad, Synthesis and structure screening of nanostructured chromium oxide powders, J. Alloys Compd., 482 (2009) 302–307.
[19] S. Balamurugan, A.L. Philip, R. Vidya, A Versatile combustion synthesis and properties of nickel oxide (NiO) nanoparticles, J. Supercond. Novel Magn., 29 (2016) 2207–2212.
[20] D. Ahire, G. Patil, G. Jain, V. Gaikwad, Synthesis of Nanostructured NiO by Hydrothermal Route and its Gas Sensing Properties, 2012 Sixth International Conference on Sensing Technology (ICST), IEEE, Kolkata, India, 2012, pp. 136–141.
[21] J.-F. Li, X. Bo, L.-J. Du, Y. Rong, T.D. Liang, Preparation of nano-NiO particles and evaluation of their catalytic activity in pyrolyzing cellulose, J. Fuel Chem. Technol., 36 (2008) 42–47.
[22] S. Sudhasree, A. Shakila Banu, P. Brindha, G.A. Kurian, Synthesis of nickel nanoparticles by chemical and green route and their comparison in respect to biological effect and toxicity, Toxicol. Environ. Chem., 96 (2014) 743–754.
[23] R. Karthiga, B. Kavitha, M. Rajarajan, A. Suganthi, Photocatalytic and antimicrobial activity of NiWO4 nanoparticles stabilized by the plant extract, Mater. Sci. Semicond. Process., 40 (2015) 123–129.
[24] J. Sharma, P. Srivastava, G. Singh, M.S. Akhtar, S. Ameen, Biosynthesized NiO nanoparticles: potential catalyst for ammonium perchlorate and composite solid propellants, Ceram. Int., 41 (2015) 1573–1578.
[25] S. Banerjee, M.C. Chattopadhyaya, Adsorption characteristics for the removal of a toxic dye, tartrazine from aqueous solutions by a low cost agricultural by-product, Arabian J. Chem., 10 (2017) S1629–S1638.
[26] C.P. Bergmann, F.M. Machado, Carbon Nanomaterials as Adsorbents for Environmental and Biological Applications, Springer, 2015.
[27] A.A. Inyinbor, F.A. Adekola, G.A. Olatunji, Kinetics, isotherms and thermodynamic modeling of liquid phase adsorption of Rhodamine B dye onto *Raphia hookerie* fruit epicarp, Water Resour. Ind., 15 (2016) 14–27.
[28] H.K. Boparai, M. Joseph, D.M. O'Carroll, Kinetics and thermodynamics of cadmium ion removal by adsorption onto nano zerovalent iron particles, J. Hazard. Mater., 186 (2011) 458–465.
[29] J.C. Igwe, A.A. Abia, Adsorption kinetics and intraparticulate diffusivities for bioremediation of Co(II), Fe(II) and Cu(II) ions from waste water using modified and unmodified maize cob, Int. J. Phys. Sci., 2 (2007) 119–127.
[30] É.C. Lima, M.A. Adebayo, F.M. Machado, Kinetic and Equilibrium Models of Adsorption, C.P. Bergmann, F.M. Machado, Eds., Carbon Nanomaterials as Adsorbents for Environmental and Biological Applications, Springer, 2015, pp. 33–69.
[31] S. Farias, D. de Oliveira, A. Souza, S. Souza, A. Morgado, Removal of reactive blue 21 and reactive red 195 dyes using

horseradish peroxidase as catalyst, Braz. J. Chem. Eng., 34 (2017) 701–707.
[32] S.K. Chaudhuri, L. Malodia, Biosynthesis of zinc oxide nanoparticles using leaf extract of Calotropis gigantea: characterization and its evaluation on tree seedling growth in nursery stage, Appl. Nanosci., 7 (2017) 501–512.
[33] S.M. Bairagi, P. Ghule, R. Gilhotra, Pharmacology of Natural Products: An Recent Approach on *Calotropis gigantea* and *Calotropis procera*, 2018.
[34] P.K. Pattnaik, D. Kar, H. Chhatoi, S. Shahbazi, G. Ghosh, A. Kuanar, Chemometric profile & antimicrobial activities of leaf extract of *Calotropis procera* and *Calotropis gigantea*, Nat. Product Res., 31 (2017) 1954–1957.
[35] J.K. Sharma, M.S. Akhtar, S. Ameen, P. Srivastava, G. Singh, Green synthesis of CuO nanoparticles with leaf extract of *Calotropis gigantea* and its dye-sensitized solar cells applications, J. Alloys Compd., 632 (2015) 321–325.
[36] M. Venigalla, Phytochemical Screening of Leaf Extracts of *Calotropis gigantea* Linn, 2009.
[37] N. Ramamurthy, S. Kannan, Fourier transform infrared spectroscopic analysis of a plant (*Calotropis gigantea* Linn) from an industrial village, Cuddalore dt, Tamilnadu, India, Romanian J. Biophys., 17 (2007) 269–276.
[38] F. Farzaneh, S.H. Kashanie, Green synthesis and characterization of Ni/NiO magnetic nanoparticles in water, J. Ceram. Process. Res., 14 (2013) 673–676.
[39] F. Thema, E. Manikandan, A. Gurib-Fakim, M. Maaza, Single phase bunsenite NiO nanoparticles green synthesis by *Agathosma betulina* natural extract, J. Alloys Compd., 657 (2016) 655–661.
[40] S. Meenakshi, N. Viswanathan, Identification of selective ion-exchange resin for fluoride sorption, J. Colloid Interface Sci., 308 (2007) 438–450.
[41] A. Asfaram, M. Ghaedi, S. Agarwal, I. Tyagi, V.K. Gupta, Removal of basic dye Auramine-O by ZnS: Cu nanoparticles loaded on activated carbon: optimization of parameters using response surface methodology with central composite design, RSC Adv., 5 (2015) 18438–18450.
[42] J.C. Igwe, A. Abia, Sorption kinetics and intrapaticulate diffusivity of As(III) bioremediation from aqueous solution, using modified and unmodified coconut fiber, Ecletica Quimica, 31 (2006) 23–29.
[43] M. Ciopec, A. Negrea, L. Lupa, C. Davidescu, P. Negrea, Studies regarding As(V) adsorption from underground water by Fe-XAD8-DEHPA impregnated resin. Equilibrium sorption and fixed-bed column tests, Molecules, 19 (2014) 16082–16101.
[44] M. Rashad, H.A. Al-Aoh, Promising adsorption studies of bromophenol blue using copper oxide nanoparticles, Desal. Water Treat., 139 (2019) 360–368.
[45] E.-S. El-Ashtoukhy, N.K. Amin, O. Abdelwahab, Removal of lead (II) and copper (II) from aqueous solution using pomegranate peel as a new adsorbent, Desalination, 223 (2008) 162–173.
[46] M. Rafiee, M. Jahangiri-rad, Adsorption of Reactive Blue 19 from aqueous solution by carbon nano tubes: equilibrium, thermodynamics and kinetic studies, Res. J. Environ. Sci., 8 (2014) 205–214.
[47] A. Angel Ezhilarasi, J. Judith Vijaya, K. Kaviyarasu, L. John Kennedy, R.J. Ramalingam, H.A. Al-Lohedan, Green synthesis of NiO nanoparticles using *Aegle marmelos* leaf extract for the evaluation of in-vitro cytotoxicity, antibacterial and photocatalytic properties, J. Photochem. Photobiol., B, 180 (2018) 39–50.
[48] S. Rakshit, S. Ghosh, S. Chall, S.S. Mati, S. Moulik, S.C. Bhattacharya, Controlled synthesis of spin glass nickel oxide nanoparticles and evaluation of their potential antimicrobial activity: a cost effective and eco friendly approach, RSC Adv., 3 (2013) 19348–19356.
[49] A.K. Ramasami, M. Reddy, G.R. Balakrishna, Combustion synthesis and characterization of NiO nanoparticles, Mater. Sci. Semicond. Process., 40 (2015) 194–202.